Title

Random Copolymers Allow Control of Crystallization and Microphase Separation in Fully Conjugated Block Copolymers

Journal

Macromolecules, 51(21)

ISSN

0024-9297

Authors

Lee, Youngmin
Aplan, Melissa P
Seibers, Zach D
et al.

Publication Date

2018-11-13

DOI

10.1021/acs.macromol.8b01859

Peer reviewed

Random Copolymers Allow Control of Crystallization and Microphase Separation in Fully Conjugated Block Copolymers

Youngmin Lee,[†,^] Melissa P. Aplan,[†] Zach D. Seibers,[‡] Renxuan Xie,[†] Tyler E. Culp,[†] Cheng Wang,[§] Alexander Hexemer,[§] S. Michael Kilbey, II,[‡,∥] Qing Wang,[⊥] and Enrique D. Gomez*[,†,#]

[†]Department of Chemical Engineering, The Pennsylvania State University, University Park, Pennsylvania 16802, United States

[‡]Department of Chemistry, University of Tennessee, Knoxville, Tennessee 37996, United States

[§]Advanced Light Source, Lawrence Berkeley National Laboratory, Berkeley, California 94720, United States

[∥]Department of Chemical and Biomolecular Engineering, University of Tennessee, Knoxville, Tennessee 37996, United States

[⊥]Department of Materials Science and Engineering, The Pennsylvania State University, University Park, Pennsylvania 16802, United States

[#]Materials Research Institute, The Pennsylvania State University, University Park, Pennsylvania 16802, United States

ABSTRACT: Thin films of fully conjugated donor−acceptor block copolymers composed of an electron donating block and an electron accepting block can be used as single component photoactive layers in organic photovoltaic (OPV) devices. In order to realize their full potential, control over microphase separation and thin-film morphology are critical. In conjugated block copolymer systems where one or more blocks can crystallize, the morphological evolution is governed by the competition between microphase separation and crystallization. In this work, we control crystallization of fully conjugated block copolymers with a random copolymer block. We suppress the crystal packing of poly(3-hexylthiophene-2,5-diyl) (P3HT) through the insertion of a small number of 3-octylthiophene (3OT) units within the chains, yielding poly(3-hexylthiophene-2,5-diyl-*random*-3-octylthiophene-2,5-diyl) (P[3HT-*r*-3OT]). While crystallization of P3HT dominates the morphology and prevents microphase separation in poly(3-hexylthiophene-2,5-diyl)-*block*-poly((9,9-dioctylfluorene-2,7-diyl)-*alt*-(4,7-di(thiophene-2-yl)-2,1,3-benzothiadiazole)-5′,5″-diyl) (P3HT-*b*-PFTBT), modest levels of 3OT suppress crystallization in P[3HT-*r*-3OT]-*b*-PFTBT, and permit microphase separation. Thus, we demonstrate that incorporating a random copolymer into a donor−acceptor block copolymer can increase control over microphase separation and lead to enhanced performance in OPV devices.

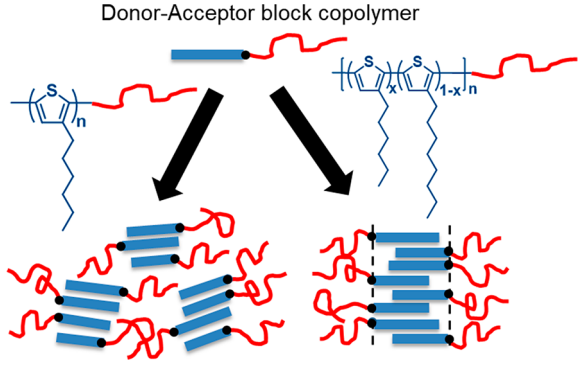

INTRODUCTION

Fully conjugated donor−acceptor block copolymers consist of covalently linked electron-donating and electron-accepting blocks. Incorporating the electron donor and the electron acceptor within the same polymer chain enables the use of donor−acceptor block copolymers as a single-component photoactive layer in organic solar cells.[1−6] Unlike the kinetically trapped structure of physical blends of electron donor and electron acceptor polymers or small molecules used in electronic devices,[7−22] the microstructure[23−26] of donor−acceptor block copolymer films can be dictated by thermodynamic equilibrium.[1−6,27−33] This microphase separation yields domains with length scales on the order of the exciton diffusion length in organic materials.[34−36] As a consequence, donor−acceptor block copolymers are a promising approach to control phase separation either in single-component active layers[1,2] or as surfactants for donor−acceptor systems.[6,37−39]

In order to realize the full potential of donor−acceptor block copolymers, controlling the thin-film morphology and microphase separation is key. Nevertheless, in fully conjugated donor−acceptor block copolymers that incorporate semicrystalline polymers, morphology control is challenging and often dominated by polymer crystallization. In previous reports, fully conjugated block copolymers incorporating various combinations of alkyl thiophenes[40,41] and selenophenes,[42] fluorene,[31] and diketopyrrolopyrrole[43] derivatives have been prepared. We propose that due to the strong tendency of poly(3-akylthiophene)s to crystallize, characteristic fibril-like crystal structures[44,45] appear in the thin-film morphology of conjugated block copolymers, rather than microphase-separated structures.

Control of crystallization is required to facilitate microphase separation in block copolymers because crystallization and microphase separation compete as the thin film morphology develops. This is exemplified in the behavior of polyethylene-*block*-poly(styrene-*r*-ethylene-*r*-butene) copolymers. In these materials, microphase separation dominates the behavior, rather than crystallization of the polyethylene block, when the interblock segregation strength (the product of the Flory–Huggins interaction parameter and the degree of polymerization, χN) is sufficiently high, about three times the interblock segregation strength at the order–disorder transition. Thus, when this criterion is met, crystallization is confined within microphase-separated domains. In contrast, when the segregation strength is low, crystallization breaks out of the microphase-separated domains and dominates the morphology of the block copolymer.[46]

This concept has also been demonstrated in rod–coil block copolymers containing one semiflexible, semicrystalline block and one flexible, amorphous block, including poly(3-hexylthiophene-2,5-diyl)-*block*-poly(2-vinylpyridine),[47,48] poly(3-dodecylthiophene-2,5-diyl)-*block*-poly(methyl methacrylate),[49] poly(3-hexylthiophene-2,5-diyl)-*block*-poly(perylene bisimide acrylate),[50,51] and poly(3-(2′-ethyl)hexylthiophene)-*block*-polylactide.[52] In these rod–coil block copolymers, various microphase-separated morphologies, including spheres, cylinders, and lamellae, are observed only when the composition of the block copolymer is dominated by the flexible block. When the composition of the block copolymer is dominated by the rod-like block, no microphase separation is observed; instead, crystallization of the stiff block dominates the morphology and prevents microphase separation.

Nevertheless, when the crystallization of the semicrystalline block is sufficiently reduced, or when the interblock segregation strength is sufficiently high, microphase separation can be observed, even when the rod-like block dominates the composition. Introduction of regiodefects in the P3HT block of P3HT-*block*-poly(2-vinylpyridine) copolymers can lead to suppressed P3HT crystallization and enhanced microphase separation.[53] P3HT-*block*-poly(perylene bisimide acrylate) prepared with a high enough molecular weight (19.7 kg/mol) of P3HT exhibits confined crystallization within microphase-separated domains.[50,51] When the side chains of poly(3-akylthiophene) are adjusted to branched ethylhexyl chains, crystallization of poly(3-(2′-ethyl)hexylthiophene) is less intense (compared to P3HT), and hexagonally packed cylinders are observed, even when the copolymer is composed mostly of the semicrytalline block.[52]

This type of manipulation of the alkyl side chain is a common approach used to control the crystallization of poly(3-akylthiophene)s and resultant properites.[54−58] Monomers with side chains of different length,[56] branching,[57] and fluorination[58] have been used to disrupt and, therefore, control the crystal packing of poly(3-akylthiophene)s. For example, in random copolymers of 3-butylthiophene and 3-octylthiophene, the interlayer stacking distance and melting temperature depend linearly on the composition of the random copolymers.[56] In random copolymers of 3-hexylthiophene and 3-(2′-ethyl)hexylthiophene, the crystal structure of the copolymer follows that of the majority component, and in contrast to the crystal structure, the melting temperature decreases gradually as more 3-(2′-ethyl)hexylthiophene is incorporated in the copolymer.[57] Alternating copolymers synthesized using 3-alkylthiophene and 3-semifluoroalkylthiophene comonomers have a bilayer lamellar crystal structure, where the bilayer lamellae are composed of alternating backbone/alkyl side chain and backbone/semifluoroalkyl side chain domains.[58]

In this work, we demonstrate an approach to control crystallization in fully conjugated block copolymers by incorporating a random copolymer as one of the blocks. We synthesize a series of random copolymers based on poly(3-hexylthiophene-2,5-diyl) (P3HT) incorporating various amounts of 3-octylthiophene (3OT). These random copolymers are incorporated into a donor–acceptor block copolymer with PFTBT, yielding poly(3-hexylthiophene-2,5-diyl-*random*-3-octylthiophene-2,5-diyl)-*block*-poly((9,9-dioctylfluorene-2,7-diyl)-*alt*-(4,7-di(thiophene-2-yl)-2,1,3-benzothiadiazole)-5′,5″-diyl) (P[3HT-*r*-3OT]-*b*-PFTBT), and the composition of the random copolymer allows the crystallinity of the P[3HT-*r*-3OT] block to be tuned. The combination of soft X-ray scattering and rheology demonstrates the presence of microphase separation, and we relate morphology in the active layer to the power conversion efficiencies of solar cell devices incorporating the donor–acceptor block copolymers as single-component photoactive materials.

MATERIALS AND METHODS

Synthesis of P[3HT-r-3OT] Macroreagent. Poly(3-hexylthiophene-2,5-diyl-*random*-3-octylthiophene-2,5-diyl) P[3HT-*r*-3OT]) was prepared in an effort to tune the crystallization of the block copolymers. A reactor charged with 2,5-dibromo-3-hexyl thiophene (Sigma-Aldrich, 97%; 2.4 g, 7.36 mmol) was evacuated for 2 min and backfilled with argon. Anhydrous THF (Acros Organics, 99.9%; 6 mL) was injected while purging the system with argon. Next, the reactor was cooled to 0 °C, and a solution containing isopropyl magnesium chloride/lithium chloride complex (Sigma-Aldrich, 1.3 M in THF; 5.4 mL, 6.99 mmol) was injected dropwise. The metal–halogen exchange reaction was allowed to proceed as the reactor was warmed to room temperature and left to react for a total of 3 h. At the same time and following the same procedure, the analogous reaction using 2,5-dibromo-3-octyl thiophene instead of 2,5-dibromo-3-hexylthiophene was prepared in a separate reactor. After 3 h were allowed for metal–halogen exchange, 2-bromo-5-chloromagnesio-3-octylthiophene (either 0.147 or 0.368 mmol) was transferred via syringe to the reactor containing 2-bromo-5-chloromagnesio-3-hexylthiophene. An additional 40 mL of THF were added to dilute the reaction mixture. A total of 1.2 mol % of [1,3-bis(diphenylphosphino)propane]dichloronickel(II) ($Ni(dppp)Cl_2$) was dissolved in 5 mL of THF. Polymerization was initiated by injecting the catalyst via syringe; the reaction was allowed to proceed for 20 min at room temperature. The polymerization was terminated by injecting 3 mL of 5 M HCl. The reaction mixture was precipitated in chilled methanol and subsequently purified by sequential Soxhlet extractions with methanol, acetone, and hexane. The random P[3HT-*r*-3OT] copolymers are referred to as P3HT(x), where x corresponds to the mole percent 3HT.

Synthesis of P[3HT-r-3OT]-*b*-PFTBT Block Copolymer. Poly(3-hexylthiophene-2,5-diyl-*random*-3-octylthiophene-2,5-diyl)-*block*-poly((9,9-dioctylfluorene-2,7-diyl)-*alt*-(4,7-di(thiophene-2-yl)-2,1,3-benzothiadiazole)-5′,5″-diyl) (P[3HT-*r*-3OT]-*b*-PFTBT) block copolymers were prepared using a chain extension reaction from the synthesized P3HT(x) macroreagents. A chain extension from the P3HT block was achieved by a Suzuki-Miyaura polycondensation reaction to grow the PFTBT block. A 100 mL Schlenk flask was charged with either P3HT(1.0), P3HT(0.98), or P3HT(0.95) (120 mg), 9,9-dioctylfluorene-2,7-diboronic acid bis(1,3-propanediol) (F; Sigma-Aldrich, 97%; 150 mg), 4,7-bis(5-bromo-2-thienyl)-2,1,3-benzothiadiazole (TBT; Sigma-Aldrich, ≥ 99.0%; 100 mg), and anhydrous toluene (Sigma-Aldrich, 99.8%; 16 mL). The headspace of the reactor was purged for 10 min with argon, after which

tetramethylammonium hydroxide solution (Sigma-Aldrich, 20 wt % in H_2O; 5 mL), tetrakis(triphenylphosphine)palladium(0) ($Pd(PPh_3)_4$; Sigma-Aldrich, 99%; 21 mg), and a few drops of Aliquat 336 (Sigma-Aldrich) were added. The reaction mixture was degassed with three freeze−pump−thaw cycles and finally backfilled with argon. The Schlenk flask was immersed in an oil bath controlled to 90 °C and the polymerization was allowed to proceed for 20 h. The reaction was terminated by injecting of bromobenzene (3 mL). The aqueous phase was separated and discarded and the organic phase was precipitated in chilled methanol. The crude product was redissolved in toluene and heated to 90 °C for 12 h, at which point it was precipitated again into chilled methanol and subsequently purified by sequential Soxhlet extractions with methanol, acetone, and hexane. The block copolymers are referred to as P3HT(x)-*b*-PFTBT.

Polymer Characterization. Molar mass distribution of all synthesized polymers was determined relative to polystyrene standards using an Agilent Technologies gel permeation chromatograph (GPC; Agilent 1260 with a ResiPore 300 × 7.5 mm column) equipped with a refractive index detector (RID). Chlorobenzene (40 °C, 1 mL/min) was used as the mobile phase. In addition, the molar mass and regioregularity of P3HTs (P3HT(x) copolymers) and the composition were calculated by ^{1}H NMR analysis using a Bruker 500 MHz instrument (Avance III HD500). Deuterated chloroform was used as the solvent.

The incorporation of 3OT into the synthesized P[3HT-*r*-3OT] was confirmed by matrix-assisted laser desorption/ionization time-of-flight mass spectrometry (MALDI-TOF MS). MALDI-TOF MS was performed using a Bruker Ultraflextreme MALDI TOF/TOF instrument equipped with 2 kHz Bruker smartbeam-II solid state laser. Poly(propylene glycol) 2700 (Sigma-Aldrich) $[M + Na]^+$ monoisotopic mass was used for external calibration. *trans*-2-[3-(4-*tert*-Butylphenyl)-2-methyl-2-propenylidene]malononitrile (DCTB; Fluka, >99%) was used as the matrix. 20 mg/mL DCTB and 10 mg/mL P3HT solutions in THF were combined as a 5:1 DCTB:P3HT ratio. Then 1 μL of the combined solution was applied to the target and allowed to dry. Mass spectra were acquired in the positive-ion reflector mode for a mass-to-charge, m/z, detection range of 700−5000 m/z. The laser sampling rate was 0.2 ns, and 2000−6000 shots were acquired for each spectrum.

Melting temperature and melting enthalpy of all synthesized polymers were determined by differential scanning calorimetry (TA Instruments Q2000) at 10 °C/min from 0 to 300 °C. To eliminate any thermal history, the second heating ramp was used for analysis.

Device Fabrication. Solar cell devices were fabricated using a conventional architecture incorporating ITO/PEDOT:PSS (70 nm)/block copolymer active layer (80−100 nm)/Al electrode (75 nm). Thickness of each layer was measured on a TENCOR P-10 surface profiler. PEDOT:PSS (Clevios P, Heraeus) was spin-cast onto ITO coated glass substrates (20 ohm/sq, Xin Yan Technology, Hong Kong) at 4000 rpm for 2 min and subsequently dried at 165 °C for 10 min. The substrate was then transferred into a nitrogen-filled glovebox (H_2O < 1 ppm and O_2 < 10 ppm) for further processing and testing. The P3HT(x)-*b*-PFTBT active layer was spin-cast using a 7.0 g/L solution of the block copolymer in chloroform at 800 rpm for 60 s. The aluminum electrode was deposited by thermal vapor deposition at 10^{-6} Torr on top of the active layer through a shadow mask (Device area = 16.2 mm^2). After cathode deposition, the devices were thermally annealed at 180 °C for 5 to 20 min to achieve optimized performance.

Photovoltaic measurements were performed on a solar simulator (Newport Model SP92250A-1000) under simulated AM 1.5G illumination (97 mW/cm^2). An optical power meter and NREL certified Si reference photocell (Newport) were used to calibrate the xenon lamp used. The current−voltage characteristics of devices were measured on a Keithley 2636A Sourcemeter under light and dark conditions.

Morphology Characterization. Morphology of block copolymer thin films was investigated using grazing-incidence wide-angle X-ray scattering (GIWAXS) and resonant soft X-ray scattering (RSoXS). GIWAXS was performed at beamline 7.3.3 of the Advanced Light Source, Lawrence Berkeley National Laboratory. Scattering data were acquired using 10.0 keV X-rays at an incident angle of 0.15°. Samples were prepared by casting PEDOT:PSS and P3HT(x)-*b*-PFTBT onto a silicon substrate following conditions used to prepare devices. Samples were thermally annealed at 180 °C in a nitrogen-filled glovebox for 10 min.

RSoXS was performed at the carbon K-edge (285.0 eV) at beamline 11.0.1.2 of the Advanced Light Source, Lawrence Berkeley National Laboratory. Samples were prepared by first depositing a layer of PEDOT:PSS onto a silicon substrate followed by P3HT(x)-*b*-PFTBT. Substrates were immersed in deionized water and as-cast films were floated off onto 5 mm × 5 mm silicon frames supporting a 1 mm × 1 mm, 100 nm thick silicon nitride window. Samples were then dried for 24 h at room temperature under vacuum and subsequently annealed at 180 °C in a nitrogen-filled glovebox for 30 min.

Transmission electron microscopy (TEM) experiments were performed on FEI Tecnai LaB6 at the Materials Characterization Lab, the Pennsylvania State University. Samples were prepared by the same procedure as those for RSoXS, except that as-cast films were floated off onto 400 mesh copper grids and annealed at 180 °C for 30 min. Films were stained by placing droplets of osmium tetroxide alongside grids in the bottom of a closed Petri dish, such that vapor staining takes place for 2 h.

Samples for rheometry are molded into 1 mm thick and 8 mm diameter pucks inside a nitrogen-filled glovebox. Samples are heated above melting and nematic clearing transitions (290 °C) under vacuum to eliminate air bubbles. Then, samples are pressed into pucks with about 1 MPa of pressure at 220 °C. Samples are loaded into a TA Instruments ARES-G2 rheometer between two 8 mm-diameter parallel plates operating under a nitrogen environment. The sample is first heated to 300 °C for 10 min to ensure good contacts and erase thermal history. Frequency sweeps from 100 to 0.1 rad/s with an oscillatory strain amplitude of 0.05 are conducted at 300 °C. Stress relaxation tests are run with a step strain of 0.05.

RESULTS AND DISCUSSION

In an effort to tune the crystallinity of P3HT, a small amount of 3OT was incorporated into the polymerization of 3HT, yielding the random copolymer P[3HT-*r*-3OT] (Scheme 1).

Scheme 1. Reaction Scheme for the Synthesis of Poly(3-hexylthiophene-2,5-diyl-*random*-3-octylthiophene2,5-diyl) (P[3HT-*r*-3OT])[a]

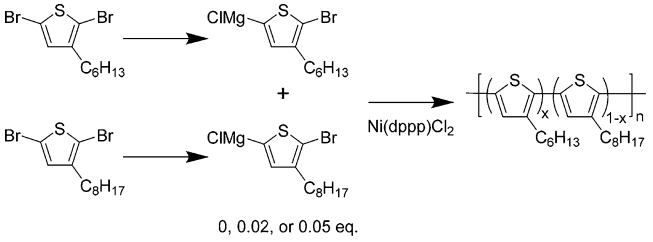

[a]The feed ratio of 3HT:3OT is controlled to produce copolymers with minor amounts of 3OT randomly enchained in the structure, which are referred to as P3HT(1.0), P3HT(0.98), and P3HT(0.95).

The synthesized batches of P[3HT-*r*-3OT] are denoted as P3HT(x) where x is the mole fraction of 3-hexylthiophene (3HT) and 1-x is the mole fraction of 3-octylthiophene (3OT) used in the polymerization.

The enchainment of 3OT to give the resultant P3HT(x) was confirmed by MALDI-TOF MS analysis. MALDI-TOF mass spectra of P3HT(1.0), P3HT(0.98), and P3HT(0.95) in the region where 13-mers to 15-mers appear are presented in Figure 1. The MALDI-TOF mass spectra (Figure 1a) of

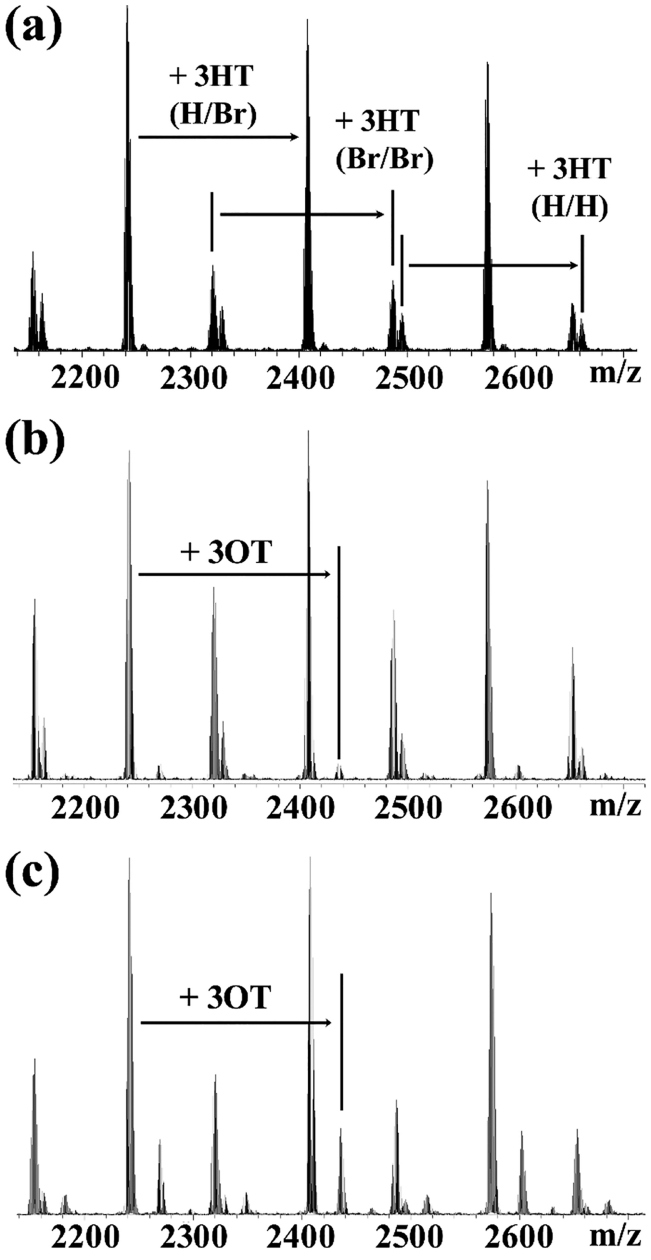

Figure 1. MALDI-TOF spectra of (a) P3HT(1.0), (b) P3HT(0.98), and (c) P3HT(0.95). Spectra confirm the addition of 3-octylthiophene into the P3HT chains, yielding P(3HT-*r*-3OT).

purified P3HT, P3HT(1.0), exhibits periodic peaks with differences in monoisotopic masses corresponding to the molar mass of the 3HT repeat unit (166.3 g/mol).[59−61] The three different peak distributions correspond to chains having different end-groups, either H/Br, H/H, or Br/Br, resulting from the GRIM mechanism. When 3OT is incorporated into the Grignard metathesis polymerization, the MADLI-TOF spectra again show the presence of chains with H/Br, H/H, and Br/Br end groups, but there also are periodic peaks corresponding to the repeat unit mass of 3OT (194.3 g/mol). The spectrum for P3HT(0.98) presented in Figure 1b shows a monoisotopic peak at m/z = 2242.5 Da, which corresponds to a P3HT 13-mer with H/Br end groups ($Br(C_{10}H_{14}S)_{13}H$; calculated monoisotopic m/z = 2242.8 Da). A small peak is also observed at m/z = 2436.7 Da (monoisotopic) corresponding to a P[3HT-*r*-3OT] 14-mer incorporating one 3OT unit in the chain and H/Br end groups: $Br-(C_{10}H_{14}S)_{13}(C_{12}H_{18}S)_1H$; calculated monoisotopic m/z = 2437.1 Da. Detailed peak assignments are shown in Table S1 of the Supporting Information. Thus, inclusion of the regiospecific monomer of 3OT with that of 3HT in the Grignard metathesis polymerization leads to a random copolymer, P[3HT-*r*-3OT]. Increasing the relative amount of 3OT used in the polymerization leads to a higher 3OT content in the resulting conjugated polymer, as seen by comparing the MALDI-TOF MS spectrum of P3HT(0.95) to that of P3HT(0.98). In all cases and as evidenced by data presented in Table 1, the addition of 3OT did not affect the regioregularity of the resulting P(3HT-*r*-3OT).

Block copolymers were prepared using P3HT(x) as a macroreagent, yielding P3HT(x)-*b*-PFTBT. GPC traces of the block copolymers and corresponding P3HT(x) macroreagents are presented in Figure S1. Block copolymers contain P3HT(x) homopolymer in the range of 10% to 21%, as shown in Figure S1 of the Supporting Information, which is consistent with previous reports of the synthesis of P3HT-*b*-PFTBT.[1,3,62] Chain extension of the macroreagents is confirmed by shifts in the elugrams toward shorter retention time after extension of the macroreagent used in the preparation of the P3HT(x)-*b*-PFTBT block copolymer. The compositions of P3HT(x)-*b*-PFTBT block copolymers are determined by analysis of ^{1}H NMR spectra, as shown in Figure S2 of the Supporting Information. The molar mass of the block copolymers is found by first determining the molecular weight of P3HT(x) from end-group analysis via NMR and then using the ratio of P3HT(x) and PFTBT to obtain the molecular weight of the second block. Number-average molecular weight, M_n, and regioregularity of P3HT(1.0), P3HT(0.98), and P3HT(0.95) are presented in Table 1 along with dispersities determined by GPC. The results show that molar mass and composition of the block copolymers are very similar throughout the series, suggesting that influences of molar mass or regioregularity of the first block (macroreagent) on the block copolymer composition are minimal. Also, the increases in M_n observed after chain extension are also very similar,

Table 1. Molar Mass, Dispersity ($Đ$), Regioregularity, and Composition of Synthesized P3HT(x) and P3HT(x)-*b*-PFTBT

	M_n (kg/mol)[a]	$Đ$[b]	regioregularity (%)[a]	weight ratio (P3HT:PFTBT)[a]
P3HT(1.0)	5.0	1.12	89	
P3HT(0.98)	6.5	1.10	92	
P3HT(0.95)	5.1	1.12	90	
P3HT(1.0)-*b*-PFTBT	7.8	1.30		64:36
P3HT(0.98)-*b*-PFTBT	9.8	1.30		66:34
P3HT(0.95)-*b*-PFTBT	8.6	1.39		59:41

[a]Determined from ^{1}H NMR. [b]Determined from GPC.

which is not unexpected given that the protocol for preparation of the block copolymer differed only by the macroreagent used.

Relative crystallinity of the block copolymer thin films was characterized using GIWAXS. 1D profiles are generated by azimuthally integrating the 2D scattering patterns and subtracting background scattering from the substrate (PEDOT:PSS/Si). All data are normalized by exposure time, thickness of films determined by ellipsometry, and weight fraction of P3HT. We can obtain an estimate of the relative crystallinity of the block copolymers by comparing the relative intensities of the peak corresponding to the (100) reflection of P3HT (Figure 2a). The intensity of the (100) peak decreases

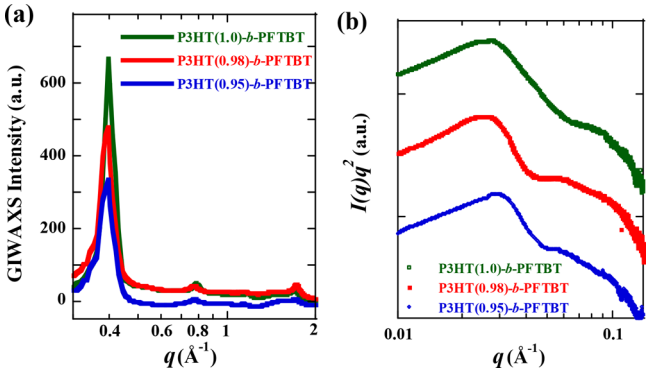

Figure 2. (a) Azimuthally integrated GIWAXS scattering profiles of P3HT(x)-*b*-PFTBT films. All data are normalized by exposure time, film thickness, and P3HT weight fraction. Background scattering from the substrate (PEDOT:PSS/Si) has also been subtracted. (b) Azimuthally integrated RSoXS scattering profiles of P3HT(x)-*b*-PFTBT films, presented as $I(q)q^2$ vs q.

as 3OT content of the P3HT(x) block increases. The same trend is observed in the azimuthally integrated scattering data of P3HT(x) homopolymers (Figure S3a of the Supporting Information). Also, in-plane and out-of-plane line cuts of block copolymer scattering data reveal the same trend as the azimuthally integrated profiles (Figure S3b,c of the Supporting Information). GIWAXS data confirms that introducing a small amount of 3OT into P3HT disrupts the crystal packing of P3HT and decreases the crystallinity within the P3HT domains in block copolymer thin films. Relative crystallinities of block copolymers were also compared based on melting enthalpies of P3HT(x) blocks obtained from DSC (see Figure S4 and Table S2 of the Supporting Information). Melting enthalpy and crystallinity decrease from P3HT(1.0) (5.9 J/g, 0.28) to P3HT(0.98) (4.8 J/g, 0.21) to P3HT(0.95) (3.8 J/g, 0.19) as 3OT was introduced as a comonomer.

Microstructure of block copolymer thin films was investigated using RSoXS. Aimuthally integrated RSoXS scattering profiles of P3HT(x)-*b*-PFTBT block copolymers are presented as $I(q)q^2$ vs q in Figure 2b and as $I(q)$ vs q in Figure S5 of the Supporting Information. Scattered intensity is generated from chemical contrast between the two blocks, resulting in the most intense peak corresponding to the average spacing between P3HT(x) and PFTBT domains. The domain spacing does not change significantly throughout the series of block copolymers examined in this work; we observe average domain spacings of 23 nm (q^* = 0.027 Å^{-1}) for P3HT(1.0)-*b*-PFTBT, 22 nm (q^* = 0.028 Å^{-1}) for P3HT(0.98)-*b*-PFTBT, and 21 nm (q^* = 0.030 Å^{-1}) for P3HT(0.95)-*b*-PFTBT. Higher order peaks are visible at $2q^*$ or 0.054 Å^{-1} for P3HT(0.98)-*b*-PFTBT and at 0.060 Å^{-1} for P3HT(0.95)-*b*-PFTBT, suggesting these copolymers adopt a lamellar morphology. In contrast, blends of P3HT and PFTBT show little evidence of structure from RSOXS profiles.[1,63] We attribute the more-defined features at high q (>0.04 Å^{-1}) to enhanced microphase separation in P3HT(0.98)-*b*-PFTBT and P3HT(0.95)-*b*-PFTBT relative to P3HT(1.0)-*b*-PFTBT, which is a direct result of the suppression of P3HT crystallization. Furthermore, Figure S6 of the Supporting Information shows bulk SAXS measurements of all three block copolymers at 260 °C, above the melting temperatures identified through DSC, where the presence of peaks suggests microphase separation.

The microstructure of block copolymer thin films was examined by TEM as shown in Figure 3. Although P3HT(1.0)-*b*-PFTBT exhibits very little that can be attributed to microphase separation, P3HT(0.98)-*b*-PFTBT and P3HT(0.95)-*b*-PFTBT show regions with significant contrast between dark and light domains that resemble a highly defective lamellar morphology.[64] Alternatively, a perforated lamellae morphology or a mixture of cylinders and lamellae is possible. Nevertheless, the enhancement in microphase separation that is apparent with addition of 3OT to the P3HT block is consistent with RSoXS results; the length scale for microphase separation (ca. 20 nm) corresponds to the average domain size obtained by RSoXS.

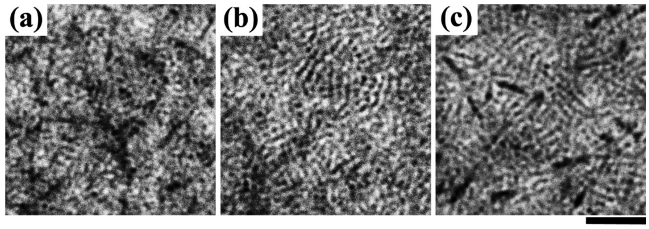

Figure 3. TEM images of P3HT(x)-*b*-PFTBT films. All films were stained by OsO_4 for 2 h. (a) P3HT(1.0)-*b*-PFTBT, (b) P3HT(0.98)-*b*-PFTBT, and (c) P3HT(0.95)-*b*-PFTBT, respectively. Scale bar = 100 nm.

The extent of microphase separation between PFTBT and P3HT blocks with different fractions of 3OT is further examined by the viscoelastic response in bulk melt rheology. Although rheology is a well-established method to probe block copolymer microphase separation,[65−67] it has only been applied to a limited extent for conjugated block copolymers.[68] Above the melting temperature and nematic-to-isotropic transition temperature of each block, rheology will yield signatures of a liquid-like response if block copolymers are disordered. Furthermore, previous work has examined the rheological response of P3HT and PFTBT homopolymers, and show that at 300 °C both polymers are isotropic and exhibit liquid-like scaling, namely $G' \approx \omega^2$ and $G'' \approx \omega$.[69,70] Figure 4a shows the storage modulus G' and loss modulus G'' as a function of frequency ω at 300 °C, where none of the block copolymers exhibit a terminal response expected of disordered (liquid-like) block copolymer chains. Thus, rheology indicates that all three block copolymers are microphase separated at 300 °C.

All P3HT(x)-*b*-PFTBT block copolymers exhibit a power-law relaxation with an exponent between 0.3 and 0.5 at small frequencies (Figure 4a). This mechanical response suggests the existence of microphase separated cylinders or lamellae,[66,67,71] and the long time stress relaxation after chain disentanglement

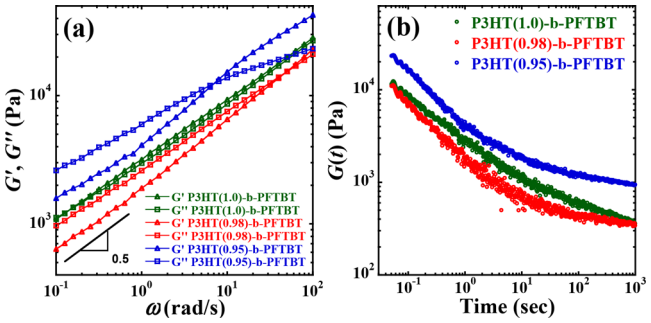

Figure 4. (a) Oscillatory frequency sweeps of P3HT(x)-*b*-PFTBT at 300 °C showing nonterminal power law behavior with exponents between 0.3 and 0.5. (b) Stress relaxation results for P3HT(x)-*b*-PFTBT at 300 °C with a step strain of 0.05.

is attributed to movement of defects at the boundary of nearby domains.[71] Figure 4b shows stress relaxation as a function of time for the three block copolymers, where P3HT(0.98)-*b*-PFTBT and P3HT(0.95)-*b*-PFTBT show a plateau in the modulus at long times. In contrast, the modulus of P3HT(1.0)-*b*-PFTBT continues to decay at times beyond 10^3 seconds. The nonterminal viscoelastic behaviors in Figures 4a and 4b are compared in Figure S7 by transforming $G(t)$ to $G'(\omega)$ and $G''(\omega)$ through the Boltzmann superposition principle. The results obtained by both oscillatory shear mode and step shear mode show reasonable match above 0.1 rad/s, and the plateau in the modulus appear again for the 3OT added block copolymers at 0.001 rad/s. We expect that at times greater than 100 s defects have explored the entire domain and the unrelaxed stress plateau for 3OT containing block copolymers may be indicative of the domain size; for P3HT(1.0)-*b*-PFTBT, we speculate that the modulus will reach a plateau lower than that of P3HT(0.98)-*b*-PFTBT at times beyond our experiment. We therefore hypothesize that at 300 °C the addition of 3OT moieties can stabilize defects in block copolymer mesophases, leading to higher moduli at long-response times with increasing 3OT content.

In order to determine the consequences of incorporating 3OT in the P3HT blocks on charge photogeneration, we fabricated solar cell devices using the various P3HT(x)-*b*-PFTBT block copolymers as single-component active layers (Figure 5 and Table 2). Photovoltaic performance of devices from each block copolymer was optimized as a function of annealing at 180 °C for times ranging from 5 to 20 min (Table S3 of the Supporting Information). Devices fabricated from P3HT(0.98)-*b*-PFTBT perform at 2.6% power conversion efficiency (PCE), which is about 20% greater than devices

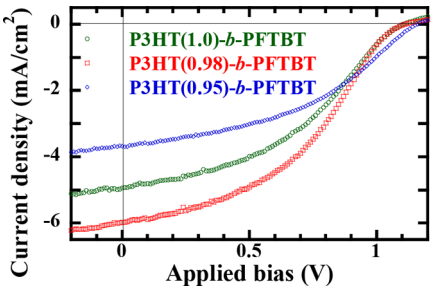

Figure 5. Characterization of photovoltaic performance of solar cell devices incorporating P3HT(x)-*b*-PFTBT films as the photoactive layer under 1 sun illumination.

Table 2. Summary of OPV Device Characteristics[a]

	PCE (%)	J_{SC} (mA/cm^2)	V_{OC} (V)	FF
P3HT(1.0)-*b*-PFTBT	2.2 ± 0.1	4.8 ± 0.2	1.09 ± 0.04	0.41 ± 0.01
P3HT(0.98)-*b*-PFTBT	2.6 ± 0.1	6.0 ± 0.1	1.12 ± 0.02	0.39 ± 0.02
P3HT(0.95)-*b*-PFTBT	1.7 ± 0.1	3.6 ± 0.2	1.15 ± 0.02	0.42 ± 0.01

[a]Uncertainty is standard deviation resulting from multiple measurements.

fabricated from P3HT(1.0)-*b*-PFTBT. The improved efficiency of devices incorporating P3HT(0.98)-*b*-PFTBT, relative to those incorporating P3HT(1.0)-*b*-PFTBT, is mainly due to an increase in short-circuit current. Differences between open-circuit voltage and fill factor of the devices are not statistically significant. An inflection point in the curves is apparent near the open-circuit voltage, which could be a result of bad contacts.[72−76] Nevertheless, because the fill factor and open-circuit voltage stay constant, we assume that contacts are equally bad across all devices. Under this assumption, it appears that enhancing microphase separation is important for maximizing the short-circuit current of solar cell devices. The same trend also appears in the performance of devices comprised of blends of P3HT(x) with PFTBT in the active layer (see Figure S8 and Table S4 of the Supporting Information). Results show that devices made using a blend of P3HT(0.98) and PFTBT outperformed devices made using blends with P3HT(1.0) and P3HT(0.95).

When the photoactive layer is composed of P3HT(0.95)-*b*-PFTBT, the power conversion efficiency decreases relative to devices fabricated from P3HT(1.0)-*b*-PFTBT and P3HT(0.98)-*b*-PFTBT. Because the introduction of a modest amount of 3OT did not significantly affect domain spacings (Figure 2), we hypothesize that crystallization of the donor block is insufficient to achieve high-performance devices, likely because charge (hole) transport is limited. Alternatively, we also consider the effects of homopolymer impurities. Previous work has demonstrated that decreasing P3HT homopolymer impurities from 56% to 19% in P3HT(1.0)-*b*-PFTBT increases performance in devices from 0.97% to 2.2% power conversion efficiency.[62] Further decreasing homopolymer impurities to 14% leads to a 2.7% efficiency when this material is used as the active layer in devices.[1,62] Comparing to results presented here, device efficiencies increase from 2.2% to 2.6% when P3HT(0.98)-*b*-PFTBT (21% homopolymer impurities) is used in the active layer instead of P3HT(1.0)-*b*-PFTBT (16% homopolymer impurities). Furthermore, P3HT(x) homopolymer impurities are lowest in P3HT(0.95)-*b*-PFTBT (10%), but devices made from this block copolymer show lower efficiencies (1.7%) than devices made from either P3HT(1.0)-*b*-PFTBT or P3HT(0.98)-*b*-PFTBT. We thus hypothesize that the differences in homopolymer impurities between 21% and 10% have a less significant impact than the tuning of crystallization of P3HT(x)-*b*-PFTBT block copolymers by the addition of 3OT moieties to the donor backbone. Overall, our work demonstrates that carefully balancing crystallization and microphase separation is critical for the performance of OPV devices incorporating fully conjugated block copolymers as the single-component active layer material.

CONCLUSIONS

Our approach demonstrates a path to achieve both crystallization and microphase separation in conjugated block copolymers, thereby balancing the need for microphase separation for mesoscale morphology control and local order for efficient charge transport. Random polymerization of comonomers in one of the blocks can suppress crystallization in fully conjugated block copolymers. By adding a small amount of 3OT to the polymerization of 3HT, we were able to carefully tune the crystallization of P3HT(x)-*b*-PFTBT thin films. While P3HT crystallization dominates the morphology of P3HT(1.0)-*b*-PFTBT films, suppressing the crystallization of P3HT in P3HT(0.98)-*b*-PFTBT enables both crystallization and microphase separation to develop. Carefully balancing the competing processes of crystallization and microphase separation led to improved device performance in solar cell devices fabricated from P3HT(0.98)-*b*-PFTBT.

AUTHOR INFORMATION

ORCID

Renxuan Xie: 0000-0001-8015-8550
S. Michael Kilbey, II: 0000-0002-9431-1138
Qing Wang: 0000-0002-5968-3235
Enrique D. Gomez: 0000-0001-8942-4480

Present Address

^Y.L.: Department of Chemical Engineering, New Mexico Tech, Socorro, New Mexico 87801, United States.

Notes

The authors declare no competing financial interest.

ACKNOWLEDGMENTS

Financial support from the Office of Naval Research under Grant N000141410532 is gratefully acknowledged. The Advanced Light Source is an Office of Science User Facility operated for the U.S. Department of Energy Office of Science by Lawrence Berkeley National Laboratory and is supported by the U.S. Department of Energy under Contract No. DE-AC02-05CH11231. Z.D.S. and S.M.K.II acknowledge support from the NSF (Award Nos. EPS 1004083 and 1512221). The authors thank Dr. Tatiana Laremore at the Penn State Proteomics and Mass Spectrometry Core Facility, University Park, PA for the help with MS data acquisition. A portion of this research was conducted at the Center for Nanophase Materials Sciences, which is a DOE Office of Science User Facility.

REFERENCES

(1) Guo, C.; Lin, Y.-H.; Witman, M. D.; Smith, K. A.; Wang, C.; Hexemer, A.; Strzalka, J.; Gomez, E. D.; Verduzco, R. Conjugated Block Copolymer Photovoltaics with near 3% Efficiency through Microphase Separation. *Nano Lett.* **2013**, *13* (6), 2957−2963.

(2) Nakabayashi, K.; Mori, H. All-Polymer Solar Cells Based on Fully Conjugated Block Copolymers Composed of Poly(3-hexylthiophene) and Poly(naphthalene bisimide) Segments. *Macromolecules* **2012**, *45* (24), 9618−9625.

(3) Guo, C.; Lee, Y.; Lin, Y.-H.; Strzalka, J.; Wang, C.; Hexemer, A.; Jaye, C.; Fischer, D. A.; Verduzco, R.; Wang, Q.; Gomez, E. D. Photovoltaic Performance of Block Copolymer Devices Is Independent of the Crystalline Texture in the Active Layer. *Macromolecules* **2016**, *49* (12), 4599−4608.

(4) Mok, J. W.; Lin, Y.-H.; Yager, K. G.; Mohite, A. D.; Nie, W.; Darling, S. B.; Lee, Y.; Gomez, E.; Gosztola, D.; Schaller, R. D.; Verduzco, R. Linking Group Influences Charge Separation and Recombination in All-Conjugated Block Copolymer Photovoltaics. *Adv. Funct. Mater.* **2015**, *25* (35), 5578−5585.

(5) Smith, K. A.; Lin, Y.-H.; Mok, J. W.; Yager, K. G.; Strzalka, J.; Nie, W.; Mohite, A. D.; Verduzco, R. Molecular Origin of Photovoltaic Performance in Donor-block-Acceptor All-Conjugated Block Copolymers. *Macromolecules* **2015**, *48* (22), 8346−8353.

(6) Mulherin, R. C.; Jung, S.; Huettner, S.; Johnson, K.; Kohn, P.; Sommer, M.; Allard, S.; Scherf, U.; Greenham, N. C. Ternary photovoltaic blends incorporating an all-conjugated donor-acceptor diblock copolymer. *Nano Lett.* **2011**, *11* (11), 4846−51.

(7) Kozub, D. R.; Vakhshouri, K.; Orme, L. M.; Wang, C.; Hexemer, A.; Gomez, E. D. Polymer Crystallization of Partially Miscible Polythiophene/Fullerene Mixtures Controls Morphology. *Macromolecules* **2011**, *44* (14), 5722−5726.

(8) Vandewal, K.; Himmelberger, S.; Salleo, A. Structural Factors That Affect the Performance of Organic Bulk Heterojunction Solar Cells. *Macromolecules* **2013**, *46* (16), 6379−6387.

(9) Benten, H.; Mori, D.; Ohkita, H.; Ito, S. Recent research progress of polymer donor/polymer acceptor blend solar cells. *J. Mater. Chem. A* **2016**, *4* (15), 5340−5365.

(10) Huang, Y.; Kramer, E. J.; Heeger, A. J.; Bazan, G. C. Bulk Heterojunction Solar Cells: Morphology and Performance Relationships. *Chem. Rev.* **2014**, *114* (14), 7006−7043.

(11) Kuei, B.; Gomez, E. D. Chain conformations and phase behavior of conjugated polymers. *Soft Matter* **2017**, *13* (1), 49−67.

(12) Kozub, D. R.; Vakhshouri, K.; Kesava, S. V.; Wang, C.; Hexemer, A.; Gomez, E. D. Direct measurements of exciton diffusion length limitations on organic solar cell performance. *Chem. Commun. (Cambridge, U. K.)* **2012**, *48*, 5859−5861.

(13) Kim, T.; Kim, J. H.; Kang, T. E.; Lee, C.; Kang, H.; Shin, M.; Wang, C.; Ma, B. W.; Jeong, U.; Kim, T. S.; Kim, B. J. Flexible, highly efficient all-polymer solar cells. *Nat. Commun.* **2015**, *6*, 8547−8553.

(14) Mao, Z.; Vakhshouri, K.; Jaye, C.; Fischer, D. A.; Fernando, R.; DeLongchamp, D. M.; Gomez, E. D.; Sauvé, G. Synthesis of Perfluoroalkyl End-Functionalized Poly(3-hexylthiophene) and the Effect of Fluorinated End Groups on Solar Cell Performance. *Macromolecules* **2013**, *46* (1), 103−112.

(15) Gao, L.; Zhang, Z. G.; Xue, L. W.; Min, J.; Zhang, J. Q.; Wei, Z. X.; Li, Y. F. All-Polymer Solar Cells Based on Absorption-Complementary Polymer Donor and Acceptor with High Power Conversion Efficiency of 8.27%. *Adv. Mater.* **2016**, *28* (9), 1884−1890.

(16) Liu, Y. H.; Zhao, J. B.; Li, Z. K.; Mu, C.; Ma, W.; Hu, H. W.; Jiang, K.; Lin, H. R.; Ade, H.; Yan, H. Aggregation and morphology control enables multiple cases of high-efficiency polymer solar cells. *Nat. Commun.* **2014**, *5*, 5293−5300.

(17) Guo, C.; Kozub, D. R.; Kesava, S. V.; Wang, C.; Hexemer, A.; Gomez, E. D. Signatures of Multiphase Formation in the Active Layer of Organic Solar Cells from Resonant Soft X-ray Scattering. *ACS Macro Lett.* **2013**, *2*, 185−189.

(18) Vakhshouri, K.; Kesava, S. V.; Kozub, D. R.; Gomez, E. D. Characterization of the mesoscopic structure in the photoactive layer of organic solar cells: A focused review. *Mater. Lett.* **2013**, *90* (0), 97−102.

(19) Yang, X.; Loos, J. Toward high-performance polymer solar cells: The importance of morphology control. *Macromolecules* **2007**, *40* (5), 1353−1362.
(20) Liu, F.; Gu, Y.; Jung, J. W.; Jo, W. H.; Russell, T. P. On the morphology of polymer-based photovoltaics. *J. Polym. Sci., Part B: Polym. Phys.* **2012**, *50* (15), 1018−1044.
(21) Ruderer, M. A.; Muller-Buschbaum, P. Morphology of polymer-based bulk heterojunction films for organic photovoltaics. *Soft Matter* **2011**, *7* (12), 5482−5493.
(22) Brabec, C. J.; Heeney, M.; McCulloch, I.; Nelson, J. Influence of blend microstructure on bulk heterojunction organic photovoltaic performance. *Chem. Soc. Rev.* **2011**, *40* (3), 1185−1199.
(23) Bates, F. S.; Fredrickson, G. H. Block copolymers - Designer soft materials. *Phys. Today* **1999**, *52* (2), 32−38.
(24) Leibler, L. Theory of microphase separation in block copolymers. *Macromolecules* **1980**, *13* (6), 1602−1617.
(25) Bates, F. S.; Fredrickson, G. H. Block copolymer thermodynamics - theory and experiment. *Annu. Rev. Phys. Chem.* **1990**, *41*, 525−557.
(26) Fredrickson, G. H.; Bates, F. S. Dynamics of block copolymers: Theory and experiment. *Annu. Rev. Mater. Sci.* **1996**, *26*, 501−550.
(27) Grieco, C.; Aplan, M. P.; Rimshaw, A.; Lee, Y.; Le, T. P.; Zhang, W.; Wang, Q.; Milner, S. T.; Gomez, E. D.; Asbury, J. B. Molecular Rectification in Conjugated Block Copolymer Photovoltaics. *J. Phys. Chem. C* **2016**, *120* (13), 6978−6988.
(28) Sun, S. S.; Zhang, C.; Ledbetter, A.; Choi, S.; Seo, K.; Bonner, C. E.; Drees, M.; Sariciftci, N. S. Photovoltaic enhancement of organic solar cells by a bridged donor-acceptor block copolymer approach. *Appl. Phys. Lett.* **2007**, *90* (4), 043117.
(29) Lin, Y. H.; Nie, W. Y.; Tsai, H. H.; Li, X. Y.; Gupta, G.; Mohite, A. D.; Verduzco, R. Supramolecular block copolymer photovoltaics through ureido-pyrimidinone hydrogen bonding interactions. *RSC Adv.* **2016**, *6* (57), 51562−51568.
(30) Mok, J. W.; Kipp, D.; Hasbun, L. R.; Dolocan, A.; Strzalka, J.; Ganesan, V.; Verduzco, R. Parallel bulk heterojunction photovoltaics based on all-conjugated block copolymer additives. *J. Mater. Chem. A* **2016**, *4* (38), 14804−14813.
(31) Verduzco, R.; Botiz, I.; Pickel, D. L.; Kilbey, S. M.; Hong, K. L.; Dimasi, E.; Darling, S. B. Polythiophene-block-polyfluorene and Polythiophene-block-poly(fluorene-co-benzothiadiazole): Insights into the Self-Assembly of All-Conjugated Block Copolymers. *Macromolecules* **2011**, *44* (3), 530−539.
(32) Gao, D.; Gibson, G. L.; Hollinger, J.; Li, P. F.; Seferos, D. S. 'Blocky' donor-acceptor polymers containing selenophene, benzodithiophene and thienothiophene for improved molecular ordering. *Polym. Chem.* **2015**, *6* (17), 3353−3360.
(33) Robb, M. J.; Montarnal, D.; Eisenmenger, N. D.; Ku, S. Y.; Chabinyc, M. L.; Hawker, C. J. A One-Step Strategy for End-Functionalized Donor-Acceptor Conjugated Polymers. *Macromolecules* **2013**, *46* (16), 6431−6438.
(34) Lee, Y.; Gomez, E. D. Challenges and Opportunities in the Development of Conjugated Block Copolymers for Photovoltaics. *Macromolecules* **2015**, *48* (20), 7385−7395.
(35) Izuhara, D.; Swager, T. M. Poly(3-hexylthiophene)-block-poly(pyridinium phenylene)s: Block Polymers of p- and n-Type Semiconductors. *Macromolecules* **2011**, *44* (8), 2678−2684.
(36) Sun, S.; Fan, Z.; Wang, Y.; Haliburton, J. Organic solar cell optimizations. *J. Mater. Sci.* **2005**, *40* (6), 1429−1443.
(37) Lombeck, F.; Sepe, A.; Thomann, R.; Friend, R. H.; Sommer, M. Compatibilization of All-Conjugated Polymer Blends for Organic Photovoltaics. *ACS Nano* **2016**, *10* (8), 8087−8096.
(38) Sivula, K.; Ball, Z. T.; Watanabe, N.; Frechet, J. M. J. Amphiphilic diblock copolymer compatibilizers and their effect on the morphology and performance of polythiophene: Fullerene solar cells. *Adv. Mater.* **2006**, *18* (2), 206−210.
(39) Lee, J. U.; Jung, J. W.; Emrick, T.; Russell, T. P.; Jo, W. H. Synthesis of C(60)-end capped P3HT and its application for high performance of P3HT/PCBM bulk heterojunction solar cells. *J. Mater. Chem.* **2010**, *20* (16), 3287−3294.
(40) Wu, P. T.; Ren, G. Q.; Li, C. X.; Mezzenga, R.; Jenekhe, S. A. Crystalline Diblock Conjugated Copolymers: Synthesis, Self-Assembly, and Microphase Separation of Poly(3-butylthiophene)-b-poly(3-octylthiophene). *Macromolecules* **2009**, *42* (7), 2317−2320.
(41) Zhang, Y.; Tajima, K.; Hashimoto, K. Nanostructure Formation in Poly(3-hexylthiophene-block-3-(2-ethylhexyl)thiophene)s. *Macromolecules* **2009**, *42* (18), 7008−7015.
(42) Hollinger, J.; Jahnke, A. A.; Coombs, N.; Seferos, D. S. Controlling Phase Separation and Optical Properties in Conjugated Polymers through Selenophene-Thiophene Copolymerization. *J. Am. Chem. Soc.* **2010**, *132* (25), 8546−8547.
(43) Ku, S. Y.; Brady, M. A.; Treat, N. D.; Cochran, J. E.; Robb, M. J.; Kramer, E. J.; Chabinyc, M. L.; Hawker, C. J. A modular strategy for fully conjugated donor-acceptor block copolymers. *J. Am. Chem. Soc.* **2012**, *134* (38), 16040−16046.
(44) Liu, J. S.; Sheina, E.; Kowalewski, T.; McCullough, R. D. Tuning the electrical conductivity and self-assembly of regioregular polythiophene by block copolymerization: Nanowire morphologies in new di- and triblock copolymers. *Angew. Chem., Int. Ed.* **2002**, *41* (2), 329−332.
(45) Kline, R. J.; McGehee, M. D.; Kadnikova, E. N.; Liu, J. S.; Frechet, J. M. J. Controlling the field-effect mobility of regioregular polythiophene by changing the molecular weight. *Adv. Mater.* **2003**, *15* (18), 1519−1523.
(46) Loo, Y. L.; Register, R. A.; Ryan, A. J. Modes of crystallization in block copolymer microdomains: Breakout, templated, and confined. *Macromolecules* **2002**, *35* (6), 2365−2374.
(47) Dai, C. A.; Yen, W. C.; Lee, Y. H.; Ho, C. C.; Su, W. F. Facile synthesis of well-defined block copolymers containing regioregular poly(3-hexyl thiophene) via anionic macroinitiation method and their self-assembly behavior. *J. Am. Chem. Soc.* **2007**, *129* (36), 11036−11038.
(48) Kim, J. S.; Kim, Y.; Kim, H. J.; Kim, H. J.; Yang, H.; Jung, Y. S.; Stein, G. E.; Kim, B. J. Regioregularity-Driven Morphological Transition of Poly(3hexylthiophene)-Based Block Copolymers. *Macromolecules* **2017**, *50* (5), 1902−1908.
(49) Moon, H. C.; Bae, D.; Kim, J. K. Self-Assembly of Poly(3-dodecylthiophene)-block-poly(methyl methacrylate) Copolymers Driven by Competition between Microphase Separation and Crystallization. *Macromolecules* **2012**, *45* (12), 5201−5207.
(50) Lohwasser, R. H.; Gupta, G.; Kohn, P.; Sommer, M.; Lang, A. S.; Thurn-Albrecht, T.; Thelakkat, M. Phase Separation in the Melt and Confined Crystallization as the Key to Well-Ordered Microphase Separated Donor-Acceptor Block Copolymers. *Macromolecules* **2013**, *46* (11), 4403−4410.
(51) Gupta, G.; Singh, C. R.; Lohwasser, R. H.; Himmerlich, M.; Krischok, S.; Muller-Buschbaum, P.; Thelakkat, M.; Hoppe, H.; Thurn-Albrecht, T. Morphology, Crystal Structure and Charge Transport in Donor-Acceptor Block Copolymer Thin Films. *ACS Appl. Mater. Interfaces* **2015**, *7* (23), 12309−12318.
(52) Ho, V.; Boudouris, B. W.; McCulloch, B. L.; Shuttle, C. G.; Burkhardt, M.; Chabinyc, M. L.; Segalman, R. A. Poly(3-alkylthiophene) Diblock Copolymers with Ordered Microstructures and Continuous Semiconducting Pathways. *J. Am. Chem. Soc.* **2011**, *133* (24), 9270−9273.
(53) Kim, J.-S.; Kim, Y.; Kim, H.-J.; Kim, H. J.; Yang, H.; Jung, Y. S.; Stein, G. E.; Kim, B. J. Regioregularity-Driven Morphological Transition of Poly(3-hexylthiophene)-Based Block Copolymers. *Macromolecules* **2017**, *50* (5), 1902−1908.
(54) Hong, X. Y. M.; Collard, D. M. Liquid crystalline regioregular semifluoroalkyl-substituted polythiophenes. *Macromolecules* **2000**, *33* (19), 6916−6917.
(55) Ho, V.; Boudouris, B. W.; Segalman, R. A. Tuning Polythiophene Crystallization through Systematic Side Chain Functionalization. *Macromolecules* **2010**, *43* (19), 7895−7899.
(56) Wu, P. T.; Ren, G. Q.; Jenekhe, S. A. Crystalline Random Conjugated Copolymers with Multiple Side Chains: Tunable Intermolecular Interactions and Enhanced Charge Transport and Photovoltaic Properties. *Macromolecules* **2010**, *43* (7), 3306−3313.

(57) Ho, V.; Beckingham, B. S.; Ng, H. H.; Segalman, R. A. Control of thermal and optoelectronic properties in conjugated poly (3-alkylthiophenes). *MRS Commun.* **2014**, *4* (2), 45−50.
(58) Wang, B.; Watt, S.; Hong, M.; Domercq, B.; Sun, R.; Kippelen, B.; Collard, D. M. Synthesis, properties, and tunable supramolecular architecture of regioregular poly(3-alkylthiophene)s with alternating alkyl and semifluoroalkyl substituents. *Macromolecules* **2008**, *41* (14), 5156−5165.
(59) Liu, J. S.; Loewe, R. S.; McCullough, R. D. Employing MALDI-MS on poly(alkylthiophenes): Analysis of molecular weights, molecular weight distributions, end-group structures, and end-group modifications. *Macromolecules* **1999**, *32* (18), 5777−5785.
(60) Kochemba, W. M.; Kilbey, S. M.; Pickel, D. L. End-group composition of poly(3-hexylthiophene)s prepared by in situ quenching of the grignard metathesis polymerization: Influence of additives and reaction conditions. *J. Polym. Sci., Part A: Polym. Chem.* **2012**, *50* (14), 2762−2769.
(61) Kochemba, W. M.; Pickel, D. L.; Sumpter, B. G.; Chen, J. H.; Kilbey, S. M. In Situ Formation of Pyridyl-Functionalized Poly(3-hexylthiophene)s via Quenching of the Grignard Metathesis Polymerization: Toward Ligands for Semiconductor Quantum Dots. *Chem. Mater.* **2012**, *24* (22), 4459−4467.
(62) Lee, Y.; Aplan, M. P.; Seibers, Z. D.; Kilbey, S. M.; Wang, Q.; Gomez, E. D. Tuning the synthesis of fully conjugated block copolymers to minimize architectural heterogeneity. *J. Mater. Chem. A* **2017**, *5* (38), 20412−20421.
(63) Grieco, C.; Aplan, M. P.; Rimshaw, A.; Lee, Y.; Le, T. P.; Zhang, W.; Wang, Q.; Milner, S. T.; Gomez, E. D.; Asbury, J. B. Molecular Rectification in Conjugated Block Copolymer Photovoltaics. *J. Phys. Chem. C* **2016**, *120* (13), 6978−6988.
(64) Eitouni, H. B.; Rappl, T. J.; Gomez, E. D.; Balsara, N. P.; Qi, S.; Chakraborty, A. K.; Frechet, J. M. J.; Pople, J. A. Signatures of the order-disorder transition in copolymers with quenched sequence disorder. *Macromolecules* **2004**, *37* (23), 8487−8490.
(65) Fredrickson, G. H.; Bates, F. S. Dynamics of Block Copolymers: Theory and Experiment. *Annu. Rev. Mater. Sci.* **1996**, *26* (1), 501−550.
(66) Kossuth, M. B.; Morse, D. C.; Bates, F. S. Viscoelastic behavior of cubic phases in block copolymer melts. *J. Rheol.* **1999**, *43* (1), 167−196.
(67) Rosedale, J. H.; Bates, F. S. Rheology of ordered and disordered symmetric poly(ethylenepropylene)-poly(ethylethylene) diblock copolymers. *Macromolecules* **1990**, *23* (8), 2329−2338.
(68) Olsen, B. D.; Teclemariam, N. P.; Muller, S. J.; Segalman, R. A. Rheological properties and the mechanical signatures of phase transitions in weakly-segregated rod-coil block copolymers. *Soft Matter* **2009**, *5* (12), 2453−2462.
(69) Xie, R.; Colby, R. H.; Gomez, E. D. Connecting the Mechanical and Conductive Properties of Conjugated Polymers. *Advanced Electronic Materials* **2018**, *4*, 1700356.
(70) Xie, R.; Lee, Y.; Aplan, M. P.; Caggiano, N. J.; Müller, C.; Colby, R. H.; Gomez, E. D. Glass Transition Temperature of Conjugated Polymers by Oscillatory Shear Rheometry. *Macromolecules* **2017**, *50* (13), 5146−5154.
(71) Rubinstein, M.; Obukhov, S. P. Power-law-like stress relaxation of block copolymers: disentanglement regimes. *Macromolecules* **1993**, *26* (7), 1740−1750.
(72) Moule, A. J.; Jung, M.-C.; Rochester, C. W.; Tress, W.; LaGrange, D.; Jacobs, I. E.; Li, J.; Mauger, S. A.; Rail, M. D.; Lin, O.; Bilsky, D. J.; Qi, Y.; Stroeve, P.; Berben, L. A.; Riede, M. Mixed interlayers at the interface between PEDOT:PSS and conjugated polymers provide charge transport control. *J. Mater. Chem. C* **2015**, *3* (11), 2664−2676.
(73) Mauger, S. A.; Li, J.; Ozmen, O. T.; Yang, A. Y.; Friedrich, S.; Rail, M. D.; Berben, L. A.; Moule, A. J. High work-function hole transport layers by self-assembly using a fluorinated additive. *J. Mater. Chem. C* **2014**, *2* (1), 115−123.
(74) Wagenpfahl, A.; Rauh, D.; Binder, M.; Deibel, C.; Dyakonov, V. S-shaped current-voltage characteristics of organic solar devices. *Phys. Rev. B: Condens. Matter Mater. Phys.* **2010**, *82* (11), 115306.
(75) Lilliedal, M. R.; Medford, A. J.; Madsen, M. V.; Norrman, K.; Krebs, F. C. The effect of post-processing treatments on inflection points in current-voltage curves of roll-to-roll processed polymer photovoltaics. *Sol. Energy Mater. Sol. Cells* **2010**, *94* (12), 2018−2031.
(76) Ecker, B.; Egelhaaf, H.-J.; Steim, R.; Parisi, J.; von Hauff, E. Understanding S-Shaped Current−Voltage Characteristics in Organic Solar Cells Containing a TiOx Interlayer with Impedance Spectroscopy and Equivalent Circuit Analysis. *J. Phys. Chem. C* **2012**, *116* (31), 16333−16337.